JOURNAL OF PROPULSION AND POWER
Vol. 21, No. 2, March–April 2005

Effect of Heat Loss on Pulse-Detonation-Engine Flow Fields and Performance

M. I. Radulescu* and R. K. Hanson†
Stanford University, Stanford, California 94305

The present study addresses the influence of convective heat losses on the flowfield and performance of pulse detonation engines (PDE). We investigate the simplest PDE configuration of a single-cycle straight detonation tube open at one end. The gasdynamics are modeled by a simple one-dimensional formulation and solved by the method of characteristics. Previous heat-flux measurements obtained in hydrogen-air and hydrogen-oxygen detonation experiments are used to calibrate the convective heat-flux model. The results are compared with previous experiments in hydrogen, propane, and ethylene mixtures with either oxygen or air. The present model is found in very good agreement with experiment and reveals how the influence of heat losses is manifested on the pressure profiles inside the detonation tube. It is shown that the nondimensional tube length *L/D*, where *D* is tube diameter, governs the amount of losses, the rate of pressure decay at the thrust wall, and hence the specific impulse. The present study reveals that the specific impulse losses vary quasi-linearly with *L/D*, reaching a deficit of approximately 20% in tube geometries of *L/D* = 50.

Nomenclature

A = $\pi D^2/4$, tube cross-sectional area
A_s = πDL, tube internal surface area subject to convective heat losses
C = c/c_{CJ}, nondimensional sound velocity
C_f = friction coefficient
C_h = heat-transfer coefficient
c = sound velocity
c_p = specific heat at constant pressure
D = tube diameter
g = gravitational acceleration
h = specific enthalpy
I_{SP} = specific impulse
L = tube length
p = pressure
Q = total energy available during one cycle inside the tube
q = heat loss rate per unit mass
$\langle \dot{q} \rangle$ = wall heat flux averaged in space and time over one cycle
q_c = heat of combustion per unit mass of mixture
R = ideal-gas constant
S = $s/\gamma R$, nondimensional entropy
s = specific entropy
T = temperature
T^0 = $\{1 + [(\gamma - 1)/2](u^2/c^2)\}T$, stagnation temperature
t = time from detonation initiation at the closed end of the tube
U = u/c_{CJ}, nondimensional particle velocity
u = particle velocity
u_w = wall velocity
V = $\pi D^2 L/4$, volume inside the tube
V_{CJ} = detonation velocity
x = distance from the closed end of the tube
β = L/D, nondimensional tube length
γ = isentropic index
ξ = x/L, nondimensional distance
ρ = gas density
τ = tc_{CJ}/L, nondimensional time

Subscripts

CJ = Chapman–Jouguet state
w = conditions at the closed wall
0 = ambient condition

Introduction

THERE is a growing popularity of utilizing detonation waves for propulsion concepts, such as the pulse detonation wave engine (PDE). A summary of the current status of PDE research can be found in Refs. 1–3. In its simplest form, a PDE consists of a straight tube open at one end, also known as a detonation tube. It is this particular simplified geometry that we are investigating in the present work. For simplicity, we are also considering a single pulse tube, as opposed to the multipulse operation that would be used in a practical device. In this configuration, after the tube is filled with a quiescent combustible gas a detonation wave initiated at the closed end propagates through the reactive mixture and exits as a strong blast wave in the surrounding atmosphere. The high-pressure products in the tube expand and exhaust the tube while the pressure in the tube decays to ambient. The propulsive performance of such a device is estimated by the generated impulse.

Such a simple geometry is easily implemented experimentally, and a significant amount of experimental data are now available.[1–3] For this reason, most modeling and theoretical work has been devoted to capture the flowfield details encountered in such a simplified geometry, estimate the generated impulse, and compare with the experimental results. In spite of these considerable efforts, typical differences in specific impulse values measured in different set of experiments and predicted by the current theoretical models differ by more than 20%. This margin is considerably larger than required to assess the viability of pulse detonation engines, based on their performance characteristics. All previous theoretical and computational studies have however neglected heat or frictional losses (e.g., see Refs. 1, 3, and 4 and references therein). Nevertheless, there has been a significant amount of experimental evidence suggesting that the dynamics of the expanding gases behind detonation waves depart significantly from the ideal isentropic profiles. Edwards' experiments were the first to correlate the effect of heat losses to the large

Presented as Paper 2004-1124 at the 42nd Aerospace Sciences Meeting and Exhibit, Reno, NV, 5–8 January 2004; received 20 April 2004; revision received 8 July 2004; accepted for publication 1 July 2004.

*Visiting Research Fellow, Mechanical Engineering Department; currently Visiting Research Fellow, Mechanical and Aerospace Engineering, Princeton University, Princeton, NJ 08544. Member AIAA.
†Professor, Mechanical Engineering Department. Fellow AIAA.

gas velocity and pressure deficits observed behind the detonation wave.[5] Edwards's pressure, velocity, and heat-flux measurements confirmed the earlier analyses of Sichel and David[6] and Skinner[7] of the influence of heat losses on the Taylor expansions behind detonation waves.[8] Similar observations on the departure of measured pressure profiles from the ideal isentropic solution were made subsequently in a number of studies.[9–11] Suspecting the possibility of heat-loss effects on PDE flowfields, Laviolette et al.[12] measured the specific impulse generated in straight detonation tubes of increasing length. Although for isentropic flow the flowfield is expected to be self-similar and invariant with geometric scaling,[4] Laviolette et al. found a significant decrease in performance with increasing tube length. They attributed these results to the increase in heat and frictional losses associated with the longer residence time of the gas in longer tubes. In a subsequent study, Kasahara et al.[13] confirmed the loss of specific impulse with tube length by conducting experiments in very long tubes. The measurements of the local heat flux and total heat load during a PDE cycle performed by Ajmani and Breisacher[14] and Hoke et al.[15] indicate that such heat losses can be comparable with the energy released in the combustion process, although the authors did not attempt to correlate these results to PDE performance parameters.

The scope of the present paper is to clarify the effect of wall heat losses on the flowfields observed behind detonation waves and on the propulsive performance of pulse detonation engines, measured by the specific impulse. Previous measurements of specific impulse in smooth detonation tubes have shown that the pressure integral on the head wall agrees within experimental accuracy (typically 5%) with measurements utilizing a ballistic pendulum,[16] which integrates all of the forces acting on the side- and endwalls. This indicates that skin friction on the side walls of the tube might have only a negligible influence on impulse in smooth wall tubes. For this reason, the present study focuses only on the effect of heat loss on the flowfields developed behind a detonation wave and the subsequent blowdown of the gases in an open tube geometry. For simplicity, we also focus on the simplest geometry consisting of a smooth wall detonation tube, for which a significant amount of experimental data are now available.

Scales and Physical Phenomena

In formulating a mathematical model for the heat-loss effects on the flowfields, we first have to consider the different physical phenomena and scales involved. Edwards studied the multidimensional fluid dynamics of the gases accelerated by the detonation waves inside tubes for conditions such that the tube diameter is much larger than the reaction zone thickness.[5–17] We are primarily concerned with the same conditions. In these previous studies, it was found that at any given instant in time the gas properties across the tube cross section are nonuniform as momentum and thermal boundary layers develop on the tube walls after passage of the detonation front. For detonations removed from marginality, the boundary layers also occupy a very small fraction of the tube cross section.[10] Although the gases in the boundary layers lose heat to the cold walls by local convection, the gases near the center of the tube are only affected by these losses gasdynamically, with a relative time delay. This delay corresponds to the time required for transverse expansion waves to reach the core of the tube and communicate the effect of heat loss from the boundary layers to the bulk of the gases. This phenomenon is well illustrated by the streak schlieren photographs taken perpendicularly to the detonation propagation direction by Edwards et al.[17] As a result of these radial expansions, the pressure and particle velocity were found to decay much more rapidly than expected from isentropic flow. These results, taken from Edwards' study[5] are shown in Figs. 1 and 2.

In general, these surface heat losses could have a noticeable influence on the detonation wave structure if transverse waves can reach the tube core before a particle has undergone its characteristic reaction time. In the present study, similar to Edwards's considerations, we are concerned with typical situations where the characteristic reaction time is much shorter than the radial expansion timescale. Because the characteristic velocity of the lateral expansion and of

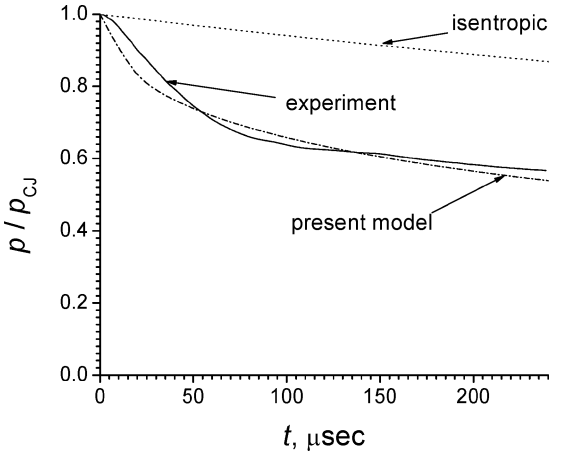

Fig. 1 Comparison between the experimental measurements of pressure behind a $2H_2 + O_2$ detonation[5] measured 8.8 m from the initiation point in a 1.6-cm-diam tube, the present model, and the Taylor isentropic solution.

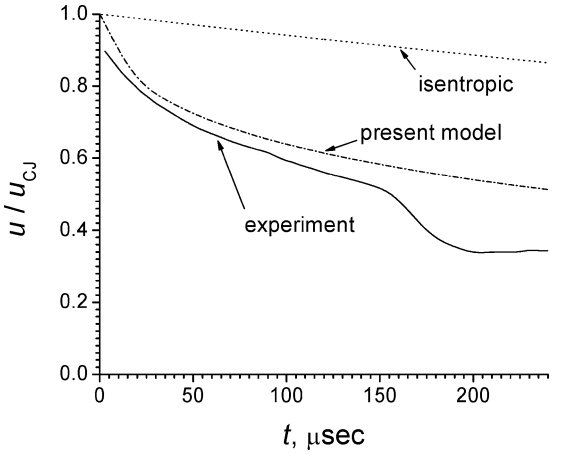

Fig. 2 Comparison between the experimental measurements of gas velocity behind a $2H_2 + O_2$ detonation[5] measured 9.7 m from the initiation point in a 1.6-cm-diam tube, the present model, and the Taylor isentropic solution.

the axial particle velocity is the same, that is, the acoustic velocity in the burned gas, our requirement is that the detonation wave thickness be much smaller than the tube diameter. This assumption is particularly valid for fuel-oxygen detonations used in previous PDE experiments, for which the reaction zone thickness (approximately a cell width) is less than a millimeter, as compared with the tube diameters, which are generally on the order of a few centimeters. Under these conditions, the boundary surface losses are communicated to the tube axis at comparatively long distances behind the Chapman–Jouguet (CJ) sonic surface. In these cases, only a small portion of the detonation wave will be affected by the surface losses, because the sonic surface isolates the reaction zone structure from the gas expansions behind the wave. Indeed, experiments have shown that the wave propagates at velocities very close to the CJ value,[18] and the properties of the gas behind the wave are well approximated by the ideal CJ state[18] (e.g., Figs. 1 and 2), although, as can be seen from Figs. 1 and 2, the expansions trailing behind the detonation front can be quite strong.

To capture the correct physical mechanism by which the heat losses influence the bulk flow downstream of the sonic surface, the two-dimensional radial relaxation process would have to be modeled. However, when the detonation tube is much longer than its diameter, that is, for $L \gg D$, the radial gasdynamic relaxation timescale (D/c) is much faster than the characteristic evolution timescale of the flowfield in the longitudinal direction (L/c). For this condition, the radial relaxation can be assumed as instantaneous. In

this case, an engineering model for the physical effect of boundary losses can be modeled via a volumetric heat-loss source term in the one-dimensional governing equations of gasdynamics, similar to Edwards et al.'s and Skinner's approaches.[5,7] This assumption signifies that the boundary losses are communicated to the entire cross section of the tube instantaneously. This one-dimensional formulation is clearly not valid close to the detonation wave front because the detonation front involves rates of energy release occurring on much faster timescales than the lateral gasdynamic relaxation, equivalent to energy removal from the bulk flow. Nevertheless, we seek this engineering approximation because we are only really interested in the dynamics of the detonation products evolving on length scales comparable with the detonation tube length, hence on much slower timescales. The CJ condition is used as a convenient boundary condition to initialize the solution. A further discussion of our engineering approximation and the boundary condition at the detonation front is discussed next.

Volumetric Source Term

In the one-dimensional formulation, the flow state variables represent average values across the detonation tube. In the presence of an energy source term per unit mass q, the one-dimensional energy equation can be written as

$$\frac{\mathrm{D}h}{\mathrm{D}t} - \frac{1}{\rho}\frac{\mathrm{D}p}{\mathrm{D}t} = T\frac{\mathrm{D}s}{\mathrm{D}t} = q \tag{1}$$

where $\mathrm{D}/\mathrm{D}t \equiv \partial/\partial t + u\partial/\partial x$ is the material derivative. The entropy formulation, also given in Eq.(1), is more convenient for the calculations.

We have performed preliminary estimates using the optically thin gas model of Ref. 19 in order to estimate whether radiative heat losses from the hot detonation products play an important role. These calculations were performed for stoichiometric ethylene-oxygen mixtures initially at ambient pressure. The model used assumes CO, CO_2, and H_2O as emitting species. Our estimates indicate that radiation losses are negligible, accounting for less than 3% of the expected peak heat fluxes caused by turbulent heat convection. For this reason, radiation losses are neglected in the present heat-loss model.

We assume that the convective volumetric source term is proportional to the temperature difference between the stagnation temperature of the mean flow and wall temperature:

$$q = -(C_h/\rho D)\left(T^0 - T_w\right)$$

$$= -(C_h/\rho D)(\{1 + [(\gamma-1)/2](u^2/c^2)\}T - T_w) \tag{2}$$

The stagnation temperature is used instead of the static temperature, in order to account for compressibility effects.[20] The stagnation temperature is equivalent to the recovery temperature for unity Prandtl number, and it takes into account the temperature increase of a fluid element caused by the adiabatic compression when the fluid velocity is decreased in the boundary layers.[20]

Similar to Edwards et al.[5] and Skinner,[7] we assume the heat-transfer coefficient C_h proportional to the heat capacity of the gas ρc_p and particle velocity difference between the gas and the wall.

$$C_h = C_f \rho c_p |u - u_w|/2 \tag{3}$$

where the wall velocity u_w is set to zero. Note that typically C_f is interpreted as the friction coefficient obtainable from Reynolds analogy between heat transfer and friction.[20] In view of the simplicity of the model used and the highly empirical nature of general turbulent boundary-layer correlations, we feel that this coefficient should be considered as a free nondimensional parameter, to be determined from appropriate experiments, rather than obtained from boundary-layer theory. For example, an accurate theory should be adjusted for the hydrodynamic turbulence generated by the cellular detonation wave structure itself[21] and the long-lived pattern of oblique shocks trailing behind the detonation front.[17] C_f is thus the only adjustable parameter of our model. For simplicity, we also assume C_f constant.

The wall temperature T_w in Eq. (2) is assumed constant and equal to ambient for the entire cycle ($T_w = 298$ K). This is not an unreasonable assumption because the heat capacity and thermal conductivities of typical PDE walls (usually steel) are large. For this reason, the temperature increase in one cycle is small[10] as compared to the temperature of the hot detonation wave products. We again stress that this assumption is mostly valid for single-pulse detonation tubes. For multiple-cycle operation of long duration, as would be encountered in PDE applications, the wall temperatures will be higher, the exact level depending on wall cooling methods.[2] Assuming that maximum temperatures of approximately 800 K would be permissible before undesirable premature ignition would occur in typical applications, we also performed some simulations with $T_w = 800$ K.

Gas Model

The gas state is assumed in quasi-equilibrium. For simplicity, we use the same formulation as developed for perfect gases. The so-called polytropic gas model used differs from the chemically frozen perfect-gas formulation by the choice of the isentropic exponent γ (Refs. 22 and 23). Instead of taking the isentropic exponent as the ratio of specific heats, we estimate it along the chemical equilibrium isentrope, that is,

$$\gamma = \left(\frac{\partial \ln P}{\partial \ln \rho}\right)_s \tag{4}$$

Under the present approximation, the sound speed and enthalpy are given by

$$c = \sqrt{\gamma(p/\rho)}, \qquad h = c^2/(\gamma - 1) \tag{5}$$

Provided the isentropic exponent does not change significantly during the gas expansion process, a constant γ approximation captures accurately the variations of enthalpy and sound velocity of a gas that is in chemical equilibrium. The validity of this approximation for PDE flowfields was discussed in Refs. 23 and 24. The present model was also compared to realistic simulations including finite rate chemical reactions in Ref. 23, where it was found that the pressure, density, particle velocity, and sound speed are very well reproduced. However, temperature is less accurate because the molar number changes are not explicitly prescribed. Nevertheless, this model provides a net overall improvement over the conventional perfect-gas and frozen chemistry assumption.

Governing Equations and Boundary Conditions

Similar to the studies of Skinner[7,26] and He and Karagozian,[25] the computations are performed in characteristic form, with the net advantage of computational speed and physical clarity. Choosing particle velocity, sound velocity, and entropy as dependent variables, the nondimensional characteristic equations for one-dimensional unsteady flow become[26,27]

$$\frac{\mathrm{D}_\pm}{\mathrm{D}\tau}\left(\frac{2}{\gamma-1}C \pm U\right) = C\frac{\mathrm{D}_\pm S}{\mathrm{D}\tau} + (\gamma-1)C\frac{\mathrm{D}S}{\mathrm{D}\tau} \tag{6}$$

$$\frac{\mathrm{D}S}{\mathrm{D}\tau} = -\beta\frac{2C_f|U|}{(\gamma-1)C^2}\left[\frac{\gamma-1}{2}U^2 + C^2 - C_0^2\right] \tag{7}$$

where

$$\frac{\mathrm{D}_\pm}{\mathrm{D}\tau} \equiv \frac{\partial}{\partial\tau} + (U \pm C)\frac{\partial}{\partial\xi}, \qquad \frac{\mathrm{D}}{\mathrm{D}\tau} \equiv \frac{\partial}{\partial\tau} + U\frac{\partial}{\partial\xi} \tag{8}$$

and Eq. (7) is the nondimensional form of Eq. (1) combined with the assumed form for the volumetric heat losses in Eq. (3). The capitalized variables refer to nondimensional quantities, and (ξ, τ) are the nondimensional space and time coordinates. These three characteristic equations given by Eqs. (6) and (7) become ordinary

differential equations along the three families of characteristics C_+, C_-, and C_0 given by

$$C_\pm : \qquad \frac{\mathrm{d}\xi}{\mathrm{d}\tau} = U \pm C \tag{9}$$

and

$$C_0 : \qquad \frac{\mathrm{d}\xi}{\mathrm{d}\tau} = U \tag{10}$$

Although we are solving for the (S, U, C) field, we are mostly interested in the pressure field. Under the assumptions of our polytropic gas model, the pressure field can be obtained from the energy equation (1) written in differential form. Using the ideal-gas law, that is, $p = \rho RT$ and Eq. (5), taking the CJ state as reference and integrating the energy equation along a particle path yields the variation of pressure with sound velocity and entropy:

$$p = p_{\mathrm{CJ}}(c/c_{\mathrm{CJ}})^{2\gamma/(\gamma-1)} \exp\{-[(s - s_{\mathrm{CJ}})/R]\}$$

$$= p_{\mathrm{CJ}} C^{2\gamma/(\gamma-1)} \exp[\gamma(S_{\mathrm{CJ}} - S)] \tag{11}$$

The governing equations (6) and (7) are integrated numerically inside the tube (i.e., for $0 \le \xi \le 1$). At the head wall (i.e., for $\xi = 1$), the velocity vanishes, and by Eq. (7) the entropy is constant, yielding

$$\xi = 0 : \qquad U = 0, \qquad S = S_{\mathrm{CJ}} \tag{12}$$

As just argued, we assume the detonation is of the CJ type, propagating at the constant CJ velocity. By virtue of the sonic CJ condition behind the wave, the detonation wave propagates along the first C_+ characteristic given by the detonation velocity itself:

$$\xi/\tau = V_{\mathrm{CJ}}/c_{\mathrm{CJ}} = U_{\mathrm{CJ}} + 1 : \qquad C = 1$$

$$U = U_{\mathrm{CJ}}, \qquad S = S_{\mathrm{CJ}} \tag{13}$$

Along this path, we assume the gas to be at the constant CJ state, as obtained from exact equilibrium calculations. Figure 3 shows the computational domain and illustrates the boundary conditions.

As already mentioned, in assigning the CJ condition immediately behind the detonation wave we have neglected the detonation wave reaction zone structure and the potential influence of losses on the detonation structure itself. Furthermore, our treatment of the boundary condition used to initialize the solution leads to a singularity on the first C_+ characteristic given by Eq. (13). From detonation wave theory, it is known that a steady sonic point can only exist if the rate of heat release is simultaneously zero.[18] This can also be seen by inspection of Eq. (6), where a constant (S, U, C) solution, such as Eq. (13), can only satisfy Eq. (6) if the rate of entropy change ($\mathrm{D}S/\mathrm{D}\tau$) is locally zero. Our numerical solution is thus equivalent of imposing a zero rate of heat release at the sonic point given by Eq. (13) and turning the losses on discontinuously on the next interior grid point. This difficulty is partially resolved by our numerical algorithm, whereby we impose the same grid spacing near the CJ surface, so that the infinitely fast relaxation, (i.e., turning "on" the heat losses) is spread out over a finite but small region consisting of the first ξ and τ steps, which were hence minimized when constructing the grid.

A strictly one-dimensional mathematically correct formulation leading to a singularity-free solution near the CJ surface would require modeling explicitly the exothermicity within the reaction zone structure and the endothermicity caused by the heat losses. For example, Ref. 28 investigated this effect of volumetric heat losses on the detonation wave structure in one dimension. This study also demonstrated that for a steady detonation solution to be possible the net rate of chemical energy addition to the flow has to vanish at the sonic point of the detonation structure. Because the heat losses are always finite, this means that a fraction of the total chemical energy is released after the sonic surface and cannot further influence the front. With increasing heat loss rates, larger fractions of the available chemical energy are lost, and the detonation wave exhibits increasing velocity deficits and could possibly be extinguished. In reality,

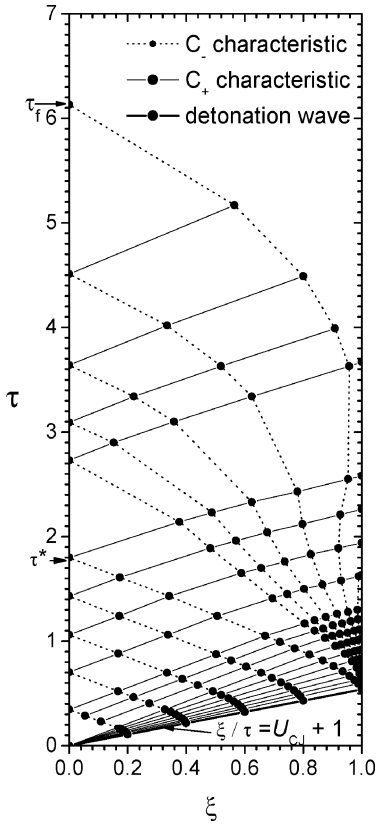

Fig. 3 Illustration of the computational domain and wave interactions obtained by the method of characteristics (computed for $C_3H_8 + 5O_2$, $P_0 = 1$ bar, $T_0 = 298$ K, $L/D = 50$); τ^* marks the end of the plateau region and τ_f the approximate arrival of a weak shock, marking the end of the computed cycle.

however, the validity of such a one-dimensional model addressing surface heat losses effects on the reaction zone structure is only applicable when the timescales of the associated lateral gasdynamic waves triggered by the surface heat losses are shorter than the reaction timescales, when the tube diameter is smaller than the reaction zone thickness, near the detonability limits. This is clearly not the case for the experiments we are trying to model in the present study, where typical reaction zone thicknesses in fuel-oxygen detonations are a few orders of magnitude thinner than the tube diameters in which they propagate.

To further validate our treatment of the numerical difficulty at the CJ surface, our numerical solution was compared with numerical simulations taking into account the effect of heat losses on the reaction zone structure in one space dimension. These results, obtained for ethylene-oxygen detonations at ambient conditions in Ref. 24, are also shown later. (See the following.) The two solutions were found in excellent agreement, although the present solution did not resolve the reaction zone structure. The solutions disagreed only during approximately 10 μs after the detonation first passed the measuring station for the example given. This corresponds to approximately 0.2% of the total time of the computation and leads to negligible errors in the time-integrated profiles.

At the open end of the detonation tube, the detonation products discharge into the surrounding gases driving a three-dimensional blast wave. This usually requires the solution of the three-dimensional flowfield outside of the tube. However, recent two-dimensional computations[25] suggest that the exit boundary condition can be well approximated one dimensionally as sonic outflow, provided the pressure near the exit of the tube is sufficiently high to accelerate the flow to the sonic condition. For lower pressures not permitting the flow acceleration to the sonic condition, the exit pressure is set to ambient. We use this one-dimensional approximation for the present computations, hence restricting the computations to the interior of the tube. The validity of this approximation is further

confirmed in the following through comparison with experimental measurements of the flowfield at the tube exit.

The six governing equations consisting of the ordinary differential equations (6), (7), (9), and (10) are written in discretized form and integrated numerically by a first-order finite difference scheme. The reader is referred to Ref. 26 for the details of the numerical algorithm. An example of the solution method is given here for the construction of a solution point in the interior domain, free from shocks and boundary interactions. Similar solutions can be derived for the various wave interactions and different boundary conditions just given. A sketch of the grid construction in (ξ, τ) space is shown in Fig. 6. The characteristic lines are assumed to be straight line segments linking two successive grid points. Starting with two given grid points 1 and 2 for which the solution is known, we seek the flow solution at point 3(S_3, U_3, C_3) and its grid location (ξ_3, τ_3). This solution grid point 3 lies on the intersection of the C_+ characteristic passing by point 1 and the C_- characteristic passing by point 2. The point 4, which is part of the solution, is the intersection between the C_0 characteristic and the line 1-3. Knowing the solution at points 1 and 2, that is, $(\xi_1, \tau_1, S_1, U_1, C_1, \xi_2, \tau_2, S_2, U_2, C_2)$, the solution at points 3 and 4, that is, $(\xi_3, \tau_3, S_3, U_3, C_3, \xi_4, \tau_4, S_4, U_4, C_4)$ satisfy the discretized version of the C_+ and C_- characteristic equations (6):

$$[2/(\gamma-1)](C_3-C_1)+(U_3-U_1)=C_{13}(S_3-S_1)$$
$$+\beta(2C_fU_{13}/C_{13})\left\{-[(\gamma-1)/2]U_{13}^2-C_{13}^2+C_0^2\right\}(\tau_3-\tau_1) \tag{14}$$

$$[2/(\gamma-1)](C_3-C_2)+(U_3-U_2)=C_{23}(S_3-S_2)$$
$$+\beta(2C_fU_{23}/C_{23})\left\{-[(\gamma-1)/2]U_{23}^2-C_{23}^2+C_0^2\right\}(\tau_3-\tau_2) \tag{15}$$

the entropy equation (7)

$$S_3-S_4=\beta\frac{2C_fU_{34}}{(\gamma-1)C_{34}^2}\left[\frac{\gamma-1}{2}U_{34}^2+C_{34}^2-C_0^2\right](\tau_3-\tau_4) \tag{16}$$

the C_+, C_- [Eq. (9)] and C_0 [Eq. (10)] characteristics

$$U_{13}+C_{13}=(\xi_1-\xi_3)/(\tau_1-\tau_3) \tag{17}$$

$$U_{23}-C_{23}=(\xi_2-\xi_3)/(\tau_2-\tau_3) \tag{18}$$

$$U_{34}=(\xi_4-\xi_3)/(\tau_4-\tau_3) \tag{19}$$

and the point 4 interpolation conditions

$$(\tau_4-\tau_1)/(\tau_4-\tau_1)=(\xi_2-\xi_1)/(\xi_2-\xi_1) \tag{20}$$

$$(S_4-S_1)/(S_4-S_1)=(\xi_2-\xi_1)/(\xi_2-\xi_1) \tag{21}$$

$$(C_4-C_1)/(C_4-C_1)=(\xi_2-\xi_1)/(\xi_2-\xi_1) \tag{22}$$

$$(U_4-U_1)/(U_4-U_1)=(\xi_2-\xi_1)/(\xi_2-\xi_1) \tag{23}$$

where a double subscript refers to average values between the respective points [e.g., $C_{13}=0.5(C_1+C_3)$]. The preceding algebraic equations can be rearranged in a suitable form and solved by an iterative procedure optimized for the form of the equations, also described in Ref. 26.

The computations were initialized at an early time along a C_- characteristic with the analytical solution for isentropic flows given by Wintenberger et al.[4] for the Taylor expansion. The integrations were stopped just before the development of a left-running shock. This weak shock follows approximately the last C_- characteristic computed and would arrive at the head wall ($\xi=0$) at the end of the cycle, raising the pressure to values very close to ambient (e.g., discussion in Ref. 29). This point marks the duration of the cycle, denoted by τ_f in Fig. 3, where the net of characteristics is illustrated for a coarse grid computation. In the region near the detonation wave front, where the strongest expansions occur, an algorithm introducing new C_+ characteristics (not shown in Fig. 3) was used in order to accurately capture the steep profiles behind the detonation wave.

Table 1 Thermochemical data for the mixtures investigated, $p_0 = 1$ bar, $T_0 = 298$ k

Mixture	s_{CJ}, kJ/kg · K	u_{CJ}, m/s	c_{CJ}, m/s	P_{CJ}, bar	γ	T_{CJ}, K
$C_3H_8+5O_2$	11.9	1088	1269	36.2	1.13	3840
C_3H_8+5 air	9.28	805	994	18.2	1.17	2810
$2H_2+O_2$	17.4	1294	1543	18.8	1.13	3680
$2H_2+$air	10.6	878	1092	15.6	1.16	2950
$C_2H_4+3O_2$	11.7	1092	1282	33.4	1.14	3930

The accuracy of the numerical solution was also checked by comparing the pressure profiles and specific impulse values obtained with different size grids and grid constructing algorithms. The results reported in the paper were obtained such that the specific impulse obtained is accurate to within approximately 0.5%.

The computations were performed for mixtures of hydrogen, propane, and ethylene with oxygen or air as oxidizer at standard initial conditions. The CJ properties required as input in the calculations were determined with the CEA equilibrium code.[30] The isentropic exponent γ was evaluated at the CJ state. A summary of the pertinent thermodynamic parameters and CJ states used to initiate the solutions is shown in Table 1.

Calibration of the Adjustable Parameter C_f

The heat-loss model was calibrated against experimental measurements of the heat flux immediately behind the detonation front in H_2/O_2 mixtures[5] and H_2/air mixtures[14] obtained using thin platinum film gauges. Using the heat-loss model just discussed, we reproduce the experimental heat-flux measurements behind the detonation wave in both studies by using

$$C_f=0.0062\pm0.0002 \tag{24}$$

The value of C_f is assumed constant for all simulations.

Using the C_f value just determined, we compared the pressure and particle profiles predicted by the preceding model with Edwards' measurements in long tubes and small diameters,[5] such that the heat losses begin to play a significant role. This permitted us to validate the present model under extreme conditions and unambiguously discriminate between the classical isentropic Taylor solution[8] and the nonisentropic solution including convective heat losses calculated in the present study. For reference, the length scale for the reaction zone in these detonations, the detonation cell width, is approximately 1 mm (Ref. 31), corresponding to a timescale of approximately 0.5 μs, which is to be compared with the 240 μs over which the profiles were measured. The comparisons in Figs. 1 and 2 reveal the validity of the present model in reproducing the correct dependence of particle velocity and pressure behind the detonation wave. In both cases, the measured and calculated profiles lie well below the ideal isentropic solution. However, the experimental particle velocity profile displays a drop near the end of its record, at approximately 140 μs. Whether this jump is real or not is unclear because the particle velocity measurements were performed using a magnetohydrodynamic method requiring a uniform distribution of the gas ionization level between the recording electrodes. Edwards et al. attribute this jump to the onset of turbulence.[5]

Scaling of the Endwall Pressure Profiles

Endwall pressure results illustrating the solution for various values of nondimensional tube length $\beta = L / D$ are shown in Fig. 7, computed for the propane-oxygen mixture. The isentropic self-similar solution obtained by setting $C_f = 0$ is also shown for comparison. For increasing values of nondimensional tube length β, the pressure is seen to decay much faster and depart from the isentropic self-similar profile. Hence, the appearance of a new characteristic length scale D, the tube diameter, governing the heat losses, breaks

the lengthwise self-similarity of the flowfield. This can be clearly seen from the governing equations, where, as first noted by Taylor,[8] the isentropic solution [by setting the right-hand side of Eqs. (6) and (7) to zero] is self-similar in the reduced time and space variables x/L and tc_{CJ}/L. Processes involving the new length scale D break the self-similarity of the solution.

One of the striking features of the nonisentropic solutions is the continuous decay of the "plateau" pressure (i.e., for $\tau < \tau^*$). The plateau time τ^* (see Fig. 3) is defined as the time elapsed before the C_- characteristics originating at the tube exit reach the end wall and "communicate" the exit condition. The plateau decay was clearly observed experimentally by Kasahara et al.[13] in their experiments in long tubes ($\beta \cong 160$), where, because of the increased losses, the pressure decayed to nearly half of its ideal value. Because of the vanishing velocity of the gas immediately near the wall, the flow is locally isentropic. The pressure decrease at the endwall is thus caused only by the arrival of the C_- expansion waves originating from the region behind the detonation wave (see Fig. 3), where the flow velocity is high, gas temperatures are high, and the losses described in the right-hand-side of Eq. (7) operate, reducing the sound velocity and hence pressure. The subsequent gas expansions occurring after the detonation exited the tube are responsible for the subsequent erosion of the head wall pressure for $\tau > \tau^*$. Because the flow is accelerated to higher velocities by the expansions originating at the tube exit, the convective heat losses and hence the strength of the expansion wave are also amplified. As a result, increasing losses leads to a more rapid decay of the endwall pressure and to more pronounced subambient excursions before the arrival of the first compression wave approximately at $\tau \cong \tau_f$.

The second remarkable feature of the governing equations and boundary conditions is the uniqueness of the solution for a constant nondimensional group (βC_f) by which experiments in different tube lengths, diameters, and boundary losses could be rescaled to yield similar results. This can be clearly seen by inspection of the governing equations and boundary conditions, whereby the source term in Eq. (7) solely dictates the deviations of the solution from the self-similar one. Because the product βC_f uniquely determines the solution, the results of Fig. 7 also illustrate graphically the sensitivity of the solution to the choice of C_f for a fixed value of β.

Comparison with Experimental Pressure Profiles

Figures 4, 5, 8 and 9 show the comparison of our simulations with the experimental pressure measurements kindly provided to us by Paul Harris. The experiments were performed in a 2.5-m tube of aspect ratio $L/D = 50$. The stoichiometric propane-oxygen mixtures were directly initiated at the closed end of the tube with an exploding wire, thus permitting direct comparison with the present calculations, which assume the instantaneous detonation formation

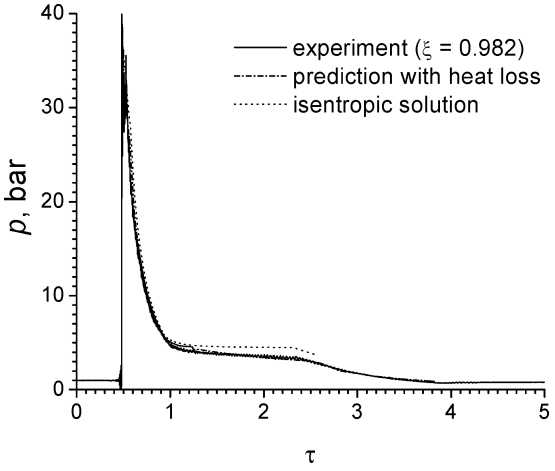

Fig. 4 Comparison between the experimental pressure profile from Harris et al.[16] and the result of the present computations for $C_3H_8 + 5O_2$ ($P_0 = 1$ bar, $T_0 = 298$ K, $\beta = L/D = 50$, $\xi = x/L = 0.982$, L = 2.5 m).

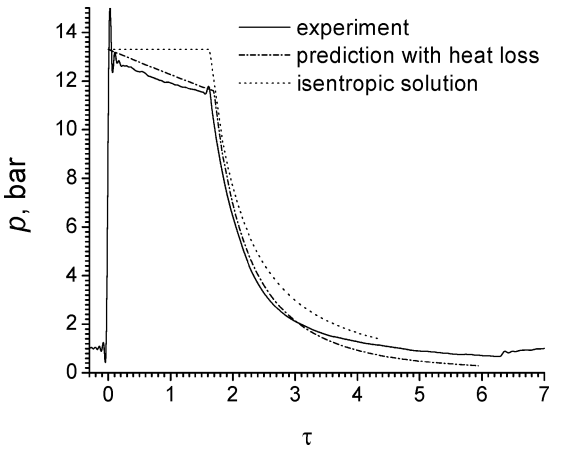

Fig. 5 Comparison between the experimental pressure profile from Harris et al.[16] obtained at the closed end of the tube and the present computations for $C_3H_8 + 5O_2$ ($P_0 = 1$ bar, $T_0 = 298$ K, $L/D = 50$, L = 2.5 m).

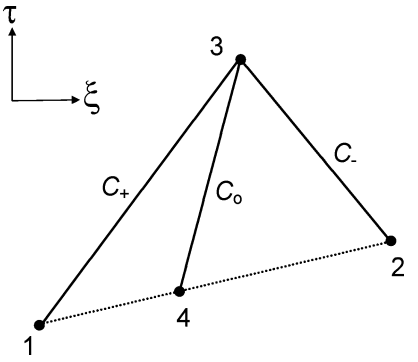

Fig. 6 Construction of the characteristics grid for an interior point.

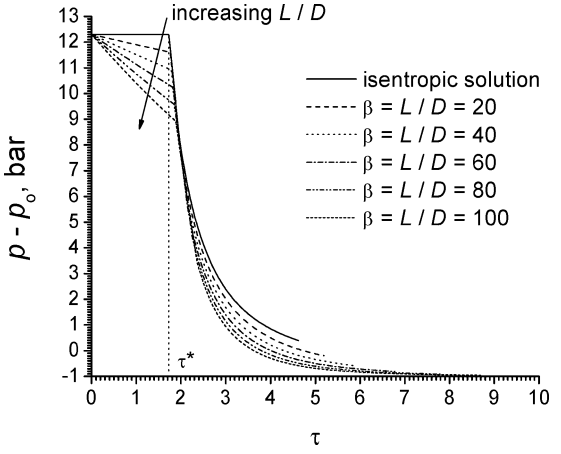

Fig. 7 Endwall pressure time histories computed for $C_3H_8 + 5O_2$ ($P_0 = 1$ bar, $T_0 = 298$ K) for various values of $\beta = L/D$.

at the head wall. The energy deposited through the ignition system (approximately 200 J) accounted for less than 0.3% of the total chemical energy released in the tube, ensuring the insignificance of the initiator on the ensuing flowfield. A detailed account of the experimental setup and technique can be found in Ref. 16.

The experimental and calculated pressures at the head wall ($\xi = 0$) are shown in Fig. 5. The pressure signal was fast-Fourier-transform filtered to eliminate the periodic pressure oscillations originating from the pointwise initiation in the finite diameter tube. These oscillations are not "noise," but rather the transverse pressure waves inside the tube whose frequency is simply determined by the tube

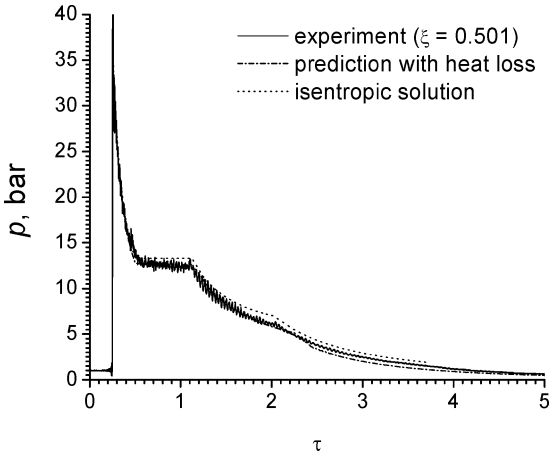

Fig. 8 Comparison between the experimental pressure profile from Harris et al.[16] and the result of the present computations for $C_3H_8 + 5O_2$ ($P_0 = 1$ bar, $T_0 = 298$ K, $\beta = L/D = 50$, $\xi = x/L = 0.501$, L = 2.5 m).

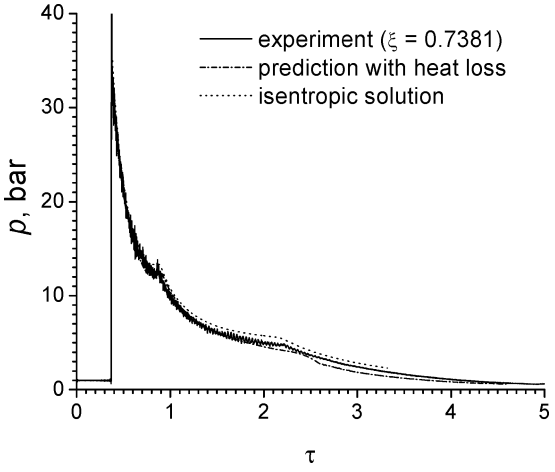

Fig. 9 Comparison between the experimental pressure profile from Harris et al.[16] and the result of the present computations for $C_3H_8 + 5O_2$ ($P_0 = 1$ bar, $T_0 = 298$ K, $\beta = L/D = 50$, $\xi = x/L = 0.7381$, L = 2.5 m).

diameter and local sound speed in the products. The agreement between the filtered experimental profile and the present model is very good. One can note that the predicted plateau pressure decay rate matches the experimental value very closely. This is not coincidental, as the same slope was reproduced in repeated experiments. Also shown is the solution obtained by setting the losses to zero. Clearly, the overall profile is better approximated by the solution incorporating heat losses, although some slight disagreement is observed at later times, when the pressure decays below ambient.

Figures 4, 8, and 9 show the pressure profiles at various locations inside the tube obtained experimentally and simulated with and without heat losses. These experimental results were not filtered, but contain the pressure oscillations inside the tube, which remain present even a long time after the detonation passed the measuring locations, indicating that the flow is most likely not laminar. These oscillations can be related to the train of oblique shocks observed by Edwards et al.[17] and Desbordes et al.[11] under similar experimental conditions. Predictions with heat losses capture the experimental profiles accurately, whereas the isentropic profiles overestimate the pressure time histories. As an example, the decaying plateau in Fig. 5 (constant in an isentropic flow) is well captured by the computations.

The excellent agreement observed for $\xi = 0.982$ (Fig. 4), very near the tube exit, confirms that the outflow boundary condition used in the present study is sufficiently accurate. To the authors' knowledge, this is the first experimental validation of such a boundary condition for PDE numerical simulations.

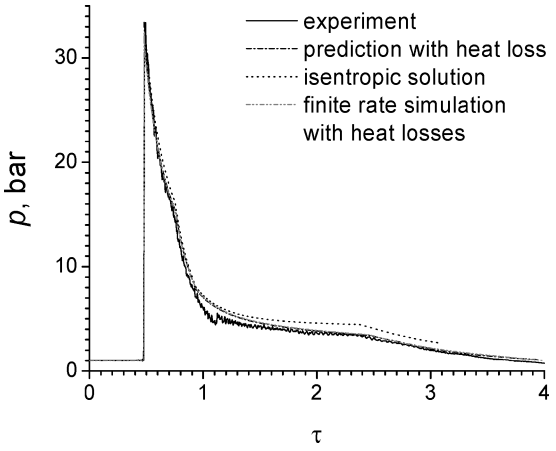

Fig. 10 Comparison between the experimental pressure profile measured in the Stanford PDE and the result of the present computations for $C_2H_4 + 3O_2$ ($P_0 = 1$ bar, $T_0 = 298$ K, $\beta = L/D = 42$, $\xi = x/L = 0.9$, $L = 1.6$ m); also shown is the computed pressure profile obtained with realistic finite-rate chemistry and treating explicitly the reaction zone structure from Ref. 24.

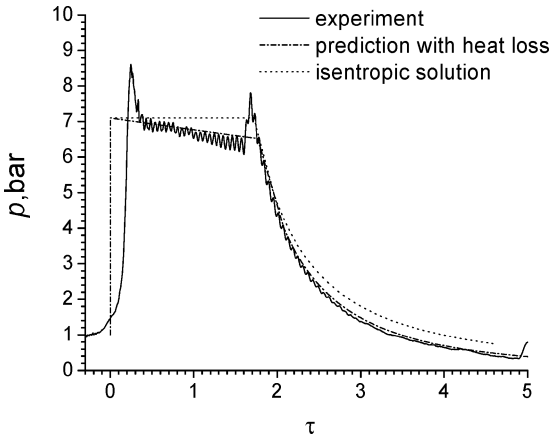

Fig. 11 Comparison between the experimental pressure profile from Kiyanda et al. (unpublished) obtained at the closed end of the tube and the present computations for $2H_2 + O_2$ ($P_0 = 1$ bar, $T_0 = 298$ K, $L/D = 33$, $L = 2.1$ m).[33]

Figure 10 shows the comparison of the simulations with experiments conducted in our laboratory in stoichiometric ethylene-oxygen, provided to us by Ethan Barbour. The Stanford detonation tube consists of a smooth tube, $L = 1.6$ m and $L/D = 42$. The experimental setup can be found in Ref. 32. The pressure–time history was recorded near the tube exit at $\xi = 0.9$. The pressure–decay history is very similar to the results obtained in propane-oxygen just presented. The heat-loss model captures well the pressure decay, whereas the isentropic model overpredicts the pressure at late times by approximately 1 bar.

Figure 11 shows the comparison of the simulations with the experimental pressure measurements provided to us by Charles Kiyanda for stoichiometric hydrogen-oxygen detonations at ambient conditions in a smooth wall tube. The details of the experimental setup can be found in Ref. 33. The tube length and aspect ratio are respectively 2.10 m and 33. For the particular experiment shown, the mixture was initiated at the closed end by a weak spark and transitioned to a detonation approximately at $\frac{1}{3}$ of the tube's length. Although the initial pressure rise caused by the delayed detonation initiation is not captured in the model, the calculation including heat losses captures very well the entire pressure decay. On the other hand, the isentropic solution significantly underpredicts the pressure decay rate.

The experimental profile of Fig. 11 displays a distinctive overshoot in pressure at the end of the pressure plateau at $\tau \approx 2$. This is

the signature of a left running weak shock, whose origin is the initial detonation wave reflection at the open end of the tube at the combustible gas/air interface. The origin of this shock is caused by the mismatch of shock impedances between the hydrogen-oxygen detonation products and the surrounding air, as predicted in Ref. 4 for hydrogen-oxygen detonations with equivalence ratios greater than 0.8. Likewise, the shock reflection analysis in Ref. 4 does not predict such a shock in hydrocarbon mixtures, consistent with experimental results.

The comparison of the simulations with the experimental pressure profiles obtained in the various mixtures has provided good agreement. For this reason, we conclude that the constant value of C_f is sufficiently accurate to reproduce the experimentally measured pressure profiles, within the accuracy of the experiments. This good agreement did not motivate us to seek higher order approximations to the value of C_f.

Effect of Heat Loss on Specific Impulse

The solutions obtained numerically were used to evaluate the specific impulse generated by the expanding detonation product gases on the end wall. The specific impulse is simply the impulse generated by the pressure force on the end wall during the duration of the exhaust process normalized by the weight of combustible mixture carried inside the tube:

$$I_{\mathrm{SP}} \equiv \frac{A\int_0^{t_f}(p_w - p_0)\,\mathrm{d}t}{\rho_0 V g} = \frac{c_0^2}{c_j g} \times \left\{ \frac{p_j}{p_0}\left[\int_0^{\tau_f} C(\xi = 0, \tau)^{2\gamma/(\gamma-1)}\,\mathrm{d}\tau\right] - \tau_f \right\} \tag{25}$$

As just described, the integration is stopped at τ_f (or the dimensional time $t_f = \tau_f L/c_j$), just before the arrival of the first left-running shock (see Fig. 3). At this point, the pressure is very near its final equilibration with ambient and includes the negative overpressure phase. The specific impulse in Eq. (25) only depends on the thermodynamic properties of the mixture and on the nondimensional solution $C(\xi = 0, \tau)$. For an isentropic solution, $C(\xi = 0, \tau)$ is uniquely determined; hence, the specific impulse is unique. For the nonisentropic flows $C(\xi = 0, \tau)$ depends uniquely on $C_f\beta$ (see preceding discussion). Hence the specific impulse is uniquely determined by $C_f\beta$.

Figures 12 and 13 compare the current computations with the experimental measurements of specific impulse obtained in smooth tubes in hydrogen-oxygen and propane-oxygen mixtures.[12,16,34] In the experiments, the specific impulse was measured using the ballistic pendulum method. The pendulum method includes the contribution of the negative overpressure phase, making our specific impulse definition appropriate for comparing the model's predictions with the experimental values. The agreement between experiment and prediction is very satisfactory considering the simplicity of the model. The numerical predictions agree both qualitatively and quantitatively with the experimental values, considering the inherent experimental difficulties in measuring the impulse with a high accuracy, typically within ±5%. For $L/D = 50$, the specific impulse loss is approximately 16–22%, with the higher losses corresponding to the hydrogen system.

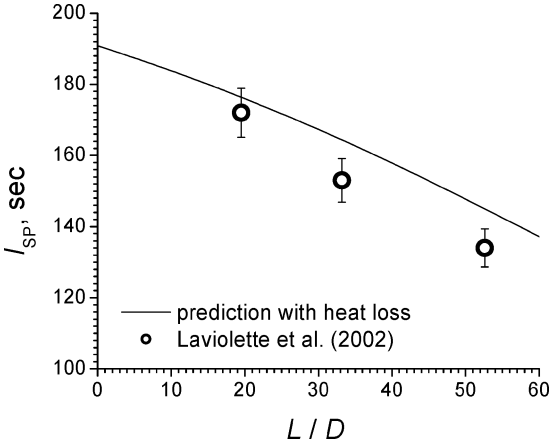

Fig. 12 Variation of specific impulse with *L/D* computed for $2H_2 + O_2$ ($P_0 = 1$ bar, $T_0 = 298$ K) and comparison with experimental values of Laviolette et al.[12]

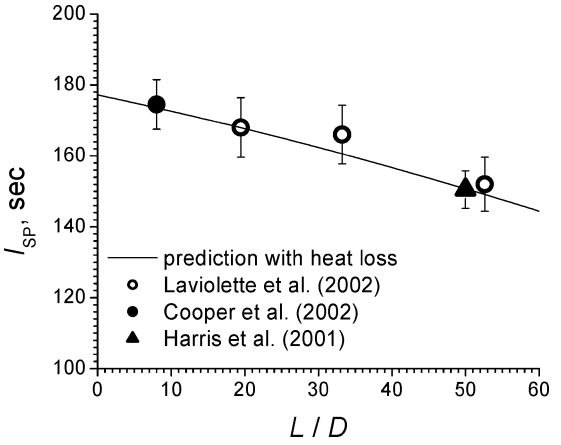

Fig. 13 Variation of specific impulse with *L/D* computed for $C_3H_8 + 5O_2$ ($P_0 = 1$ bar, $T_0 = 298$ K) and comparison with experimental values of Cooper et al.[34] and Laviolette et al.[12]

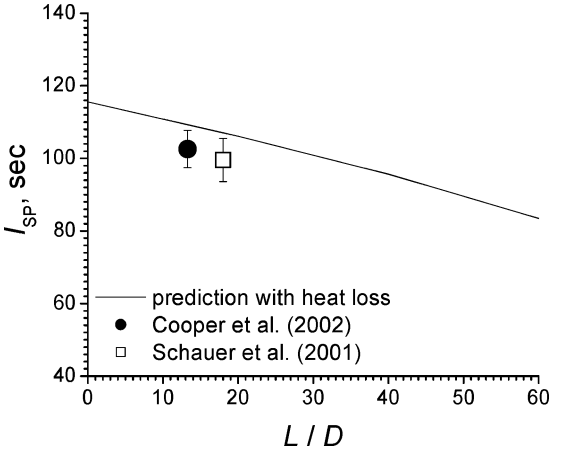

Fig. 14 Variation of specific impulse with *L/D* computed for $C_3H_8 + 5$Air ($P_0 = 1$ bar, $T_0 = 298$ K) and comparison with experimental values of Cooper et al.[34] (ballistic pendulum) and of Schauer et al.[35]

Real pulse detonation engine applications are likely to be air-breathing. Figure 14 shows the specific impulse estimated for a stoichiometric propane-air mixture. Propane-air is typical of most hydrocarbon mixtures because the energy content and reaction products of most hydrocarbon mixtures, including JP-10, are very similar.[4] Despite the fact that product temperatures in mixtures using air as the oxidizer are lower by 1000 K (see Table 1), a specific impulse deficit of 22% is observed for $L/D = 50$, as opposed to a deficit of 16% for the propane-oxygen case. This is the reverse of the expected trend, based on temperature differences alone. The same trend was verified for hydrogen-air and hydrogen-oxygen mixtures, where the losses were found greater in the air system. This effect might be caused by the higher heat of combustion in the oxygen systems, leading to effectively smaller heat losses relative to the amount of available chemical energy.

Also shown in Fig. 14 are the experimental results of Refs. 34 and 35. The agreement between experiment and simulation is quite good, in view of the nonidealities in the experiments and simplifications in the present model.

Dilution of the fuel-oxygen mixtures with nitrogen (to obtain air) is equivalent to studying fuel-oxygen mixtures diluted with

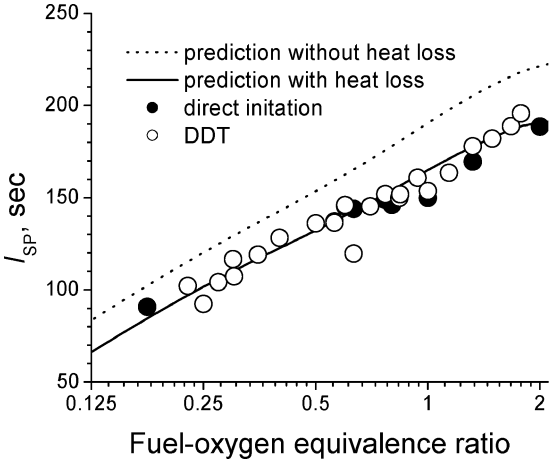

Fig. 15 Variation of specific impulse for H_2-O_2 mixtures ($P_0 = 1$ bar, $T_0 = 298$ K) and varying equivalence ratio from Kiyanda et al.[33] and comparison with the present model.

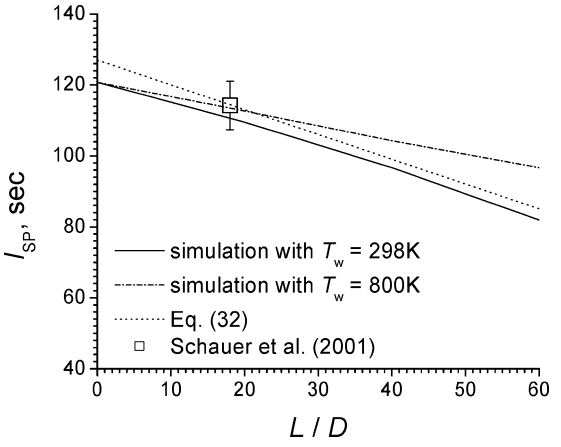

Fig. 16 Variation of specific impulse with *L/D* computed for $2H_2$ + Air ($P_0 = 1$ bar, $T_0 = 298$ K) for $T_w = 298$ and 800 K, comparison with Eq. (31) in the text and the experimental data of Schauer et al.[35] obtained by the thrust stand technique in multicycle experiments.

excess fuel or excess oxygen. Kiyanda et al. did an extensive study to measure the specific impulse in hydrogen-oxygen mixtures as a function of fuel-oxygen equivalence ratio.[33] Their experiments focused on both deflagration-to-detonation transition and direct initiation of the detonations waves, where the same impulse was found irrespective of the initiation mode, demonstrating that the PDE impulse is only governed by energy considerations. The experiments were performed in a detonation tube with $L/D = 33$ and $L = 2.1$ m. A comparison of the present model with their experimental data is shown in Fig. 15. Our model with heat loss is found in excellent agreement with the experimental data over the entire range of equivalence ratios for which a detonation wave was initiated inside the tube, suggesting that the constant C_f model is sufficiently accurate.

So far, we have discussed the ideal performance of single-pulse detonation tubes for which the wall temperature was set to ambient, that is, 298 K. In real applications, however, the wall temperature is likely to increase and be prevented from overheating by some cooling method.[2] To assess the importance of heat losses in more realistic scenarios, we set the wall temperature to 800 K. This value represents a reasonable upper bound for permissible wall temperatures to prevent premature gas autoignition upon injection in the tube. The results of these simulations are shown in Fig. 16 for the hydrogen-air system. Also shown are the experimental results of Schauer et al.,[35] obtained in a multipulse facility of $L/D = 18$. The 800 K wall temperature simulation leads to a specific impulse deficit at $L/D = 50$ of 17%, as compared to the 26% deficit for $T_w = 298$ K. The difference is attributed to the smaller temperature differences in the hot wall scenario, which are responsible for the smaller local heat fluxes.

Energetic Considerations

The results of the computations and the experimental data shown in Figs. 12–16 also indicate that the specific impulse losses vary almost linearly with increasing L/D. This finding is of practical importance in PDE design considerations. This approximate relationship can be alternatively derived from energetic considerations. Kiyanda et al.[33] showed that the performance of a PDE can be simply correlated with the total chemical heat release in a given mixture, irrespective of the details of the gasdynamic flowfields, yielding

$$I_{SP} \propto \sqrt{Q} \tag{26}$$

Differentiating Eq. (26), we obtain the relationship between changes in the total available energy and changes in specific impulse:

$$\mathrm{d}I_{SP}/I_{SP} = 0.5\,\mathrm{d}Q/Q \tag{27}$$

For small deviations from the ideal specific impulse, Eq. (27) yields an explicit relationship between the actual specific impulse and the total heat loss per cycle:

$$I_{SP,actual}/I_{SP,ideal} \approx 1 - 0.5(Q_{LOSS}/Q) \tag{28}$$

The maximum available energy Q can be written in terms of the heat of combustion per unit mass of the mixture q_c:

$$Q = \rho_0 V q_c = \rho_0 \pi (D^2 L/4) q_c \tag{29}$$

The total heat loss per cycle Q_{LOSS} can be written in terms of the average wall heat flux per cycle and the duration of the cycle:

$$Q_{LOSS} = \langle \dot{q} \rangle A_s t_f \approx \langle \dot{q} \rangle \pi D L 5 (L/c_{CJ}) \tag{30}$$

where the characteristic duration of the cycle is taken as approximately $\approx 10L/V_{CJ} \approx 5L/c_{CJ}$ (e.g., Fig. 3, and discussion in Ref. 4). Combining Eqs. (28–30), we obtain a linear dependence between the specific impulse and the aspect ratio of the tube L/D:

$$\frac{I_{SP,actual}}{I_{SP,ideal}} \approx 1 - \left[\frac{10\langle \dot{q} \rangle}{\rho_0 q_c c_{CJ}}\right]\frac{L}{D} \tag{31}$$

depending only on the thermodynamic properties of the mixture and the average wall heat flux. This relationship is useful once the average rate of wall heat flux is known or can be estimated. The functional dependence of $\dot{q}$ is given in Eq. (33). This can be used to estimate the parameters on which the second term of Eq. (31) depends. Nevertheless, because of the averaging required of the highly transient values of local heat flux $\dot{q}$(see the following), an accurate simplified quantitative expression is difficult to obtain from Eq. (31) without introducing high levels of empiricism.

Hoke et al.[15] measured the amount of heat loss in a PDE of $L/D = 18$ operating on stoichiometric hydrogen-air at a frequency of 20 Hz by using an ingenious and accurate calorimetric method. From their measurements of the total heat loss rate (21 kW) and assuming that heat loss occurs during the useful duration of the cycle (i.e., $\tau_f \approx 5$), an average wall heat flux of $\langle \dot{q} \rangle \cong 1.7$ MW/m^2 is obtained. Note that Ajmani and Breisacher[14] obtain a slightly higher time-averaged heat flux in the same mixture (2.5 kW/m^2), but their measurements are obtained from a single-shot operation, where the wall temperature is probably lower than in Hoke et al.'s experiments. Furthermore, their measurements were time averaged at a single location along the tube, whereas the values obtained from Hoke et al.'s study represents a time and space average along the entire tube length. Substituting the value derived from Hoke et al.'s study and using the thermochemical properties of stoichiometric hydrogen-air at ambient conditions ($q_c = 3.39$ MJ/kg, $\rho_0 = 0.855$ kg/m^3, $c_{CJ} = 1091.5$ m/s), we obtain the following correlation:

$$I_{SP,actual}/I_{SP,ideal} \approx 1 - 0.0055(L/D) \tag{32}$$

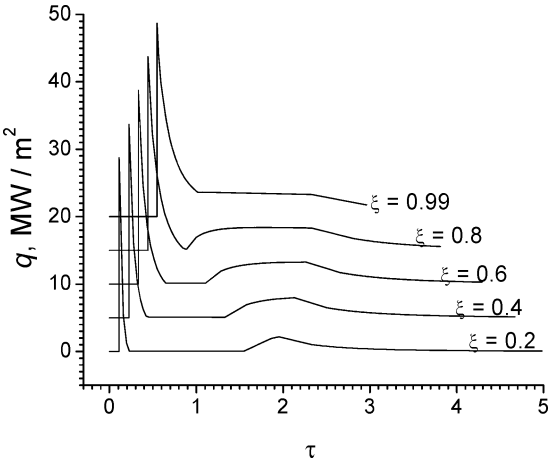

Fig. 17 Time histories of wall heat flux at different locations inside the detonation tube for $2H_2 + Air$ ($P_0 = 1$ bar, $T_0 = 298$ K, $T_w = 298$ K, $L/D = 18$); successive traces shifted up by five units for clarity.

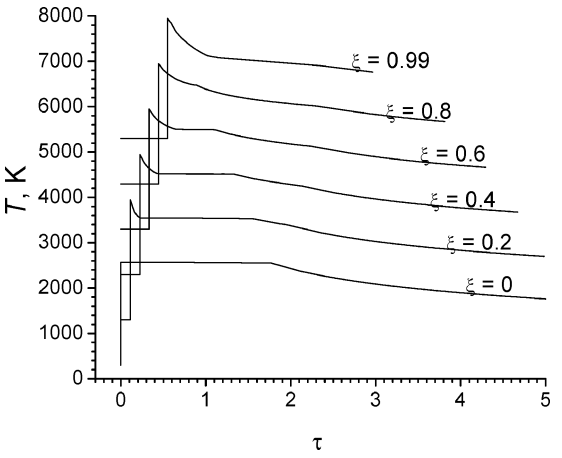

Fig. 18 Time histories of gas temperature at different locations inside the detonation tube for $2H_2 + Air$ ($P_0 = 1$ bar, $T_0 = 298$ K, $T_w = 298$ K, $L/D = 18$); successive traces shifted up by 1000 units for clarity.

valid for stoichiometric hydrogen-air mixtures in multi-cycle operations. This simple estimate is shown in Fig. 16. Note that in Eq. (32) the ideal specific impulse is not known, and only the slope of the linear dependence is explicit. Reasonable good agreement is observed between the slope of the specific impulse dependence on tube aspect ratio derived from Hoke et al.'s calorimetric measurements and the present calculations. It thus follows that the correct L/D dependence can be estimated reasonably well from energetic considerations alone, provided the average heat flux can be estimated or is known from experiment.

Further validation of our model can be achieved by comparing the predicted average wall heat flux with experimental values. Figure 17 shows the calculated distributions of wall heat flux, given by

$$\dot{q} = C_h\left(T^0 - T_w\right) = (C_f \rho c_p |u|/2) \times\left(\{1 + [(\gamma - 1)/2](u^2/c^2)\}T - T_w\right) \tag{33}$$

These were computed for a hydrogen-air mixture, with $L/D = 18$ and $T_w = 298$ K, corresponding to the PDE configuration of Schauer et al.[35] Clearly, the wall heat-flux profiles have two local maxima. The first peak, used to calibrate the C_f value, is associated with the gas immediately behind the traveling detonation wave. In this region, the products are close to CJ temperature (see Fig. 18), and the local gas velocity is also very high (see Fig. 19). The Taylor expansion wave following the detonation wave decelerates the particles to very low values, and hence the convective heat losses drop. The second peak in wall heat flux is associated with the strong expansion wave generated upon reflection of the detonation wave at the open end of the tube (see Fig. 3). The strong expansion wave reaccelerates the gas towards the open end to velocities close to 1000 m/s (Fig. 19). Although the temperature of the gas had further decayed as a result of the Taylor wave, the heat flux remains high as a result of this high gas velocity. Subsequently, the reflected strong expansion wave originating from the end wall decelerates the escaping gas, and because the gas temperature continuously drops the wall heat flux continuously decays. For completeness, the corresponding pressure profiles are shown in Fig. 20. The arrival of the various waves just described can be tracked on the $\xi - \tau$ diagram of Fig. 3 and on Figs. 17–20 as the distinctive sudden change of slopes of the various profiles.

To estimate the heat load communicated to the wall over one cycle, we estimated the time-averaged wall heat flux at various locations inside the tube. These profiles are shown in Fig. 21. Clearly, the tube experiences higher time-average values with decreasing distance from the open end. The reason for this trend can be seen directly from Fig. 17 illustrating the velocity field inside the tube. Closer to the tube exit, the gas is in motion for much longer time. Close to the endwall, the gas spends a high fraction of the cycle at very low velocities. For these reasons, the walls closer to the tube exit

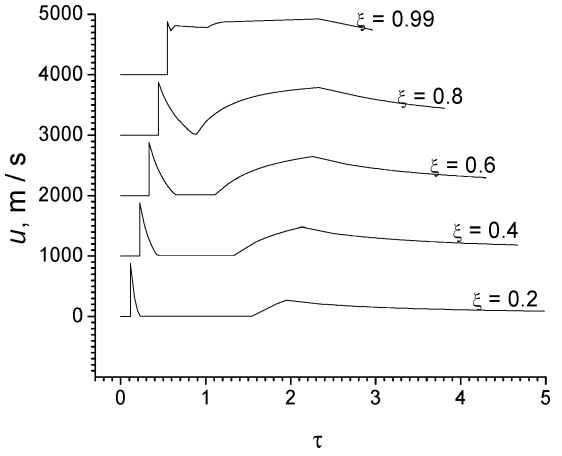

Fig. 19 Time histories of gas velocity at different locations inside the detonation tube for $2H_2 + Air$ ($P_0 = 1$ bar, $T_0 = 298$ K, $T_w = 298$ K, $L/D = 18$); successive traces shifted up by 1000 units for clarity.

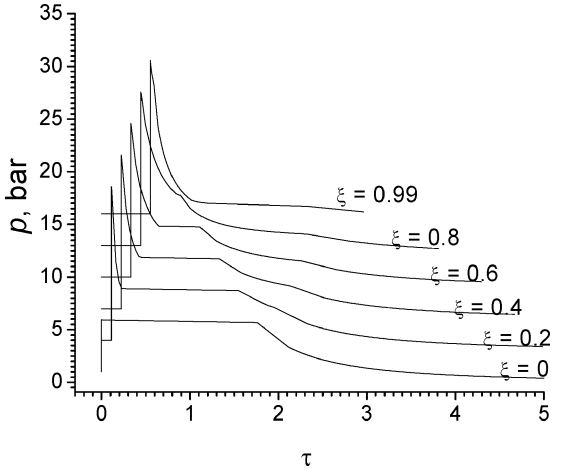

Fig. 20 Time histories of gas pressure at different locations inside the detonation tube for $2H_2 + Air$ ($P_0 = 1$ bar, $T_0 = 298$ K, $T_w = 298$ K, $L/D = 18$); successive traces shifted up by three units for clarity.

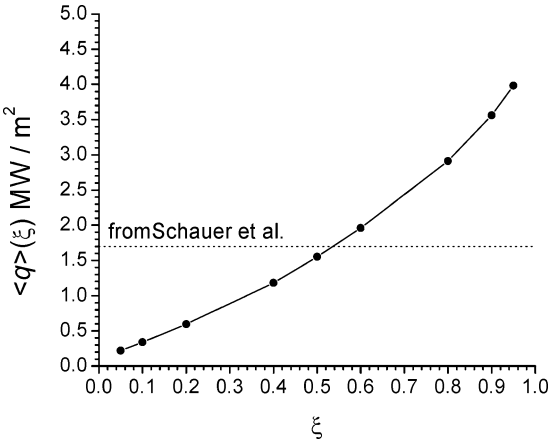

Fig. 21 Spatial distribution of time-averaged heat-flux values inside the detonation tube obtained for $2H_2 + Air$ ($P_0 = 1$ bar, $T_0 = 298$ K, $T_w = 298$ K, $L/D = 18$) and the average heat flux deduced from the calorimetric measurements of Hoke et al.[15]

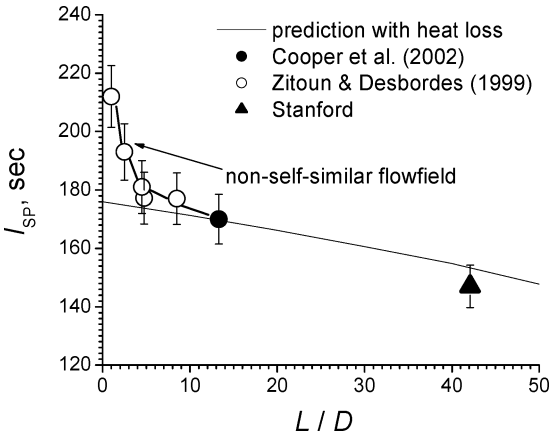

Fig. 22 Variation of specific impulse with L/D computed for $C_2H_4 + 3O_2$ ($P_0 = 1$ bar, $T_0 = 298$ K) and comparison with experimental values of Zitoun and Desbordes[36] and Barbour et al.[32] measured by integrating head wall pressure and the measurements of Cooper et al.[34] obtained by the ballistic pendulum technique.

are exposed to large heat fluxes for longer times, hence higher time-averaged heat fluxes.

The quasi-linear dependence of time-average heat flux with location inside the tube also has a very important practical implication: the cycle-average heat flux can be estimated from the time-average heat flux at the midtube location, hence simplifying the experimental task of determining the cycle-average heat flux.

For the example just considered, the cycle-average heat flux is 1.72 MW/m^2. This is in excellent agreement with the value derived from Hoke's calorimetric study[15] of 1.7 MW/m^2. Although the agreement with one experimental data point could be completely fortuitous, this result appears promising in that our simple model also captures well the average heat load per cycle in an open-ended detonation tube.

Break of Self-Similarity When $L/D \sim 1$

It was just shown that the specific impulse in an open-ended detonation tube varies quasi-linearly with L/D. One could be tempted to extrapolate the results of our model or of experimental data to small values of L/D and use this extrapolated value as an estimate for the maximum impulse that could be generated in a straight open-ended detonation tube. This would however be incorrect and would lead to a significant underestimation of the maximum performance. The reason is that for short tubes, where the tube length is on the order of the tube diameter, although heat losses become insignificant, one can no longer assume axial selfsimilarity of the flowfield. For these conditions, pressure relaxation processes across the tube diameter introduce the length scale D in the phenomenon description, hence the break in the longitudinal self-similarity of the process. At the tube exit, expansions are communicated to the gas from the tube edge radially inwards. This effectively acts as a time delay for the expansions to penetrate inside the tube. For this reason, the pressure inside the tube will be maintained higher for a longer time, hence leading to a higher value of specific impulse. This indeed accounts for the higher-than-predicted impulses observed experimentally by Zitoun and Desbordes[36] in short tubes in ethylene-oxygen mixtures (see Fig. 22). Also shown in Fig. 22 are the results obtained by Cooper et al.[34] and those obtained in our own facility[32] for larger values of L/D. As can be seen, the results of the present simulations are in good agreement with the experimental data, except for the cases where L/D approaches unity.

Further Discussion

The comparison of available experimental flowfields obtained in smooth detonation tubes and the current model yield in general very good agreement, suggesting that heat losses play an important role. It was also found that a unique value of the friction coefficient C_f in the convective heat-loss correlation, derived from experimental heat-flux measurements behind stoichiometric hydrogen-oxygen and hydrogen-air detonations, accounts for the experimental data (within experimental accuracy) available for off-stoichiometric mixtures and for hydrocarbon fuels as well. At present, this conclusion rests on limited empirical observations, and this very good agreement might seem surprising, in view of the significant idealizations of the model and the complicated physical phenomena that occur in reality (turbulent boundary layers, shock/boundary-layer interactions, self-turbulization of the flow from detonation wave instabilities, etc.). For this reason, before unequivocal acceptance of the proposed model can be obtained additional experiments are necessary to directly measure the heat-loss rates and correlate these with the properties of the turbulent detonation product gases under conditions where heat losses begin to play a significant role, such as for very large L/D ratios.

In the present study, the influence of frictional losses was not considered. The relevance of such losses, particularly in tubes where obstacles are employed, remains an open issue. Because in general such obstacles are incorporated in practical PDE implementation for less-sensitive gas mixtures in order to promote initiation, the role of increasing friction must be reevaluated. Because the obstacles also promote turbulence and hence local convective heat exchange with the detonation tube walls, the close coupling between frictional losses and heat losses needs further investigation outside the realm of idealized smooth wall detonation tubes. For example, the specific impulse obtained in tubes with internal blockages was found significantly lower[34] than in the smooth wall tubes.

Conclusions

The present study evaluated the effect of heat loss on open-ended detonation-tube flowfields and clarified the geometrical scaling of such devices. It is found that heat losses affect significantly the gas dynamics inside the tube and the impulse generated by the expanding gas. Larger heat losses were found to increase the expansion rates and hence lead to smaller impulses.

Acknowledgments

This work was sponsored by the Office of Naval Research (Gabriel Roy as technical monitor). M. Radulescu was supported by a postdoctoral fellowship from the Fonds de Recherche sur la Nature et les Technologies, Québec, Canada. The authors wish to acknowledge Andrew Higgins, Christopher Morris, and Joe Shepherd for useful discussions and Paul Harris, Charles Kiyanda, and Ethan Barbour for sharing their experimental data with us.

References

[1] Kailasanath, K., "Recent Developments in the Research on Pulse Detonation Engines," *AIAA Journal*, Vol. 41, No. 2, 2003, pp. 145–158.

[2]Bazhenova, T. V., and Golub, V. V., "Use of Gas Detonation in a Controlled Frequency Mode (Review)," *Combustion, Explosion, and Shock Waves*, Vol. 39, No. 4, 2003, pp. 365–381.

[3]Wu, Y. H., Ma, F. H., and Yang, V., "System Performance and Thermodynamic Cycle Analysis of Airbreathing Pulse Detonation Engines,"*Journal of Propulsion and Power*, Vol. 19, No. 4, 2003, pp. 556–567.

[4]Wintenberger, E., Austin, J. M., Cooper, M., Jackson, S., and Shepherd, J. E., "An Analytical Model for the Impulse of a Single-Cycle Pulse Detonation Tube," *Journal of Propulsion and Power*, Vol. 19, No. 1, 2003, pp. 22–38.

[5]Edwards, D. H., Brown, D. R., Hooper, G., and Jones, A. T., "The Influence of Wall Heat Transfer on the Expansion Following a C-J Detonation Wave," *Journal of Physics D: Applied Physics*, Vol. 3, No. 3, 1970, pp. 365–376.

[6]Sichel, M., and David, T. S., "Transfer Behind Detonations in H_2-O_2 Mixtures," *AIAA Journal*, Vol. 4, No. 6, 1966, pp. 1089, 1090.

[7]Skinner, J. H., Jr., "Friction and Heat-Transfer Effects on the Nonsteady Flow Behind a Detonation," *AIAA Journal*, Vol. 5, No. 11, 1967, pp. 2069–2071.

[8]Taylor, G. I., "The Dynamics of the Combustion Products Behind Plane and Spherical Detonation Fronts in Explosives," *Proceedings of the Royal Society of London, Series A: Mathematical and Physical Sciences A*, Vol. 200, No. 1061, 1950, pp. 235–247.

[9]Paillard, C., Dupré, G., Lisbet, R., Combourieu, J., Fokeev, V. P., Gvozdeva, L. G., and Bazhenova, T. V., "Pressure and Wall Heat Transfer Behind a Hydrogen/Azide Detonation Wave in Narrow Tubes," *Gasdynamics of Detonations and Explosions*, edited by J. R. Bowen, N. Manson, A. K. Oppenheim, and R. I. Soloukhin, Progress in Astronautics and Aeronautics, Vol. 75, AIAA, New York, 1981, pp. 135–149.

[10]Bazhenova, T. V., Fokeev, V. P., Lobastov, Yu., Brossard, J., Bonnet, T., Brion, B., and Charpentier, N., "Influence of the Nature of Confinement on Gaseous Detonation," *Gasdynamics of Detonations and Explosions*, edited by J. R. Bowen, N. Manson, A. K. Oppenheim, and R. I. Soloukhin, Progress in Astronautics and Aeronautics, Vol. 75, AIAA, New York, 1981, pp. 87–107.

[11]Desbordes, D., Manson, N., and Brossard, J., "Influence of Walls on the Pressure Behind Self-Sustained Expanding Cylindrical and Plane Detonations in Gases," *Shock Waves, Explosions, and Detonations*, edited by J. R. Bowen, N. Manson, A. K. Oppenheim, and R. I. Soloukhin, Progress in Astronautics and Aeronautics, Vol. 87, AIAA, New York, 1983, pp. 302–317.

[12]Laviolette, J. P., Kiyanda, C. B., and Higgins, A. J., "The Effect of Friction and Heat Transfer on Impulse in a Detonation Tube," Canadian Section of Combustion Institute, May 2002.

[13]Kasahara, J., Tanahashi, Y., Numata, T., Matsuo, A., and Endo, T., "Experimental Studies on L/D Ratio and Heat Transfer in Pulse Detonation," 19th International Colloquium on the Dynamics of Explosions and Reactive Systems, Paper 65, July–Aug. 2003 (on CD-ROM).

[14]Ajmani, K., and Breisacher, K. J., "Qualitative Study of Cooling Methods for a Pulse Detonation Engine," JANNAF, Chemical Propulsion Information Agency, 2002.

[15]Hoke, J., Bradley, R., and Schauer, F., "Heat Transfer and Thermal Management in a Pulsed Detonation Engine," AIAA Paper 03-6486, Jan. 2003.

[16]Harris, P. O., Farinaccio, R., Stowe, R. A., Higgins, A. J., Thibault, P. A., and Laviolette, J. P., "The Effect of DDT Distance on Impulse in a Detonation Tube," AIAA Paper 01-3467, July 2001.

[17]Edwards, D. H., Jones, T. G., and Price, B., "Observations on Oblique Shock Waves in Gaseous Detonations," *Journal of Fluid Mechanics*, Vol. 17, No. 1, 1963, pp. 21–34.

[18]Fickett, W., and Davis, C. D., *Detonation*, Univ. of California Press, Berkeley and Los Angeles, 1979, p. 55.

[19]Ju, Y., Guo, H., Liu, F., and Maruta, K., "Effects of the Lewis Number and Radiative Heat Loss on the Bifurcation and Extinction of CH_4/O_2-N_2-He flames," *Journal of Fluid Mechanics*, Vol. 379, Jan. 1999, pp. 165–190.

[20]Schlichting, H., *Boundary-Layer Theory*, McGraw–Hill, New York, 1979, p. 265.

[21]White, D., "Turbulent Structure of Gaseous Detonations," *Physics of Fluids*, Vol. 4, No. 4, 1961, pp. 465–480.

[22]Gruschka, H. D., and Wecken, F., *Gasdynamic Theory of Detonation*, Gordon and Breach, New York, 1971, p. 89.

[23]Radulescu, M. I., and Hanson, R. K., Comment on "Analytical Model for the Impulse of Single-Cycle Pulse Detonation Tube," *Journal of Propulsion and Power*, Vol. 20, No. 5, 2004, pp. 956–959.

[24]Radulescu, M. I., Morris, C. I., and Hanson, R. K., "The Effect of Wall Heat Loss on the Flow Fields in a Pulse-Detonation Wave Engine," AIAA Paper 2004-1124, Jan. 2004.

[25]He, X., and Karagozian, A. R., "Numerical Simulation of Pulse Detonation Engine Phenomena," *Journal of Scientific Computing*," Vol. 19, No. 1–3, 2003, pp. 201–223.

[26]Skinner, J. H., Jr., "Plane-Flame Simulation of the Wake Behind an Internally Propelled Vehicle—Part I—Simulation of a Supersonic Vehicle by a Detonation," Rensselaer Polytechnic Inst., TR AE 6701, Troy, NY, March 1967.

[27]Foa, J. V., *Elements of Flight Propulsion*, Wiley, New York, 1960, p. 90.

[28]Brailovsky, I., and Sivashinky, G., "Effects of Momentum and Heat Losses on the Multiplicity of Detonation Regimes," *Combustion and Flame*, Vol. 128, No. 1-2, 2002, pp. 191–196.

[29]Guzik, S. M., Harris, P. G., and De Champlain, A., "An Investigation of Pulse Detonation Engine Configurations Using the Method of Characteristics," AIAA Paper 2002-4066, July 2002.

[30]Gordon, S., and McBride, B. J., "Computer Program for Calculation of Complex Chemical Equilibrium Compositions and Applications," NASA RP-1311, Oct. 1994.

[31]Manzhalei, V. I., Mitrofanov, V. V., and Subbotin, V. A., "Measurement of Inhomogeneities of a Detonation Front in Gas Mixtures at Elevated Pressures," *Combustion Explosion Shock Waves (USSR)*, Vol. 10, No. 1, 1974, pp. 89–95.

[32]Barbour, E. A., Owens, Z. C., Morris, C. I., and Hanson, R. K., "The Impact of a Converging-Diverging Nozzle on PDE Performance and its Associated Flowfield," AIAA Paper 2004-867, Jan. 2004.

[33]Kiyanda, C. B., Tanguay, V., Higgins, A. J., and Lee, J. H. S., "Effect of Transient Gasdynamic Processes on the Impulse in Pulse Detonation Engines," *Journal of Propulsion and Power*, Vol. 18, No. 5, 2002, pp. 1124–1126.

[34]Cooper, M., Jackson, S., Austin, J., Wintenberger, E., and Shepherd, J. E., "Direct Experimental Impulse Measurements for Detonations and Deflagrations," *Journal of Propulsion and Power*, Vol. 18, No. 5, 2002, pp. 1033–1041.

[35]Schauer, F., Stutrud, J., and Bradley, R., "Detonation Initiation Studies and Performance Results for Pulsed Detonation Engines," AIAA Paper 2001-1129, Jan. 2001.

[36]Zitoun, R., and Desbordes, D., "Propulsive Performances of Pulsed Detonations," *Combustion Science and Technology*, Vol. 144, Nos. 1–6, 1999, pp. 93–114.